ORGANOMETALLICS
Article

Organometallics **2010,** *29,* 6723–6731 6723
DOI: 10.1021/om1007743

Oligomerization of Ethylene Using New Tridentate Iron Catalysts Bearing α-Diimine Ligands with Pendant S and P Donors

Brooke L. Small,*[,†] Ray Rios,[†] Eric R. Fernandez,[†] Deidra L. Gerlach,[‡] Jason A. Halfen,[‡] and Michael J. Carney[‡]

[†]*Chevron Phillips Chemical Company, 1862 Kingwood Drive, Kingwood, Texas 77339, United States, and* [‡]*Department of Chemistry, University of Wisconsin−Eau Claire, 105 Garfield Avenue, Eau Claire, Wisconsin 54702, United States*

Received August 9, 2010

Stoichiometric Schiff base condensations of sterically bulky primary amines with acenaphthenequinone yield isolable monoimines. In the presence of iron(II) chloride, the remaining ketone reacts with a second primary amine bearing a pendant donor atom to give asymmetric, tridentate, α-diimine complexes that possess remarkable structural variability. A series of NNP and NNS tridentate iron(II) complexes are prepared; these coordination compounds become active catalysts for ethylene oligomerization when activated with methylalumoxanes. X-ray crystallographic studies of the precatalyst complexes confirm that the ligand binds in a tridentate fashion. Correlations between the precatalyst solid-state structures and catalyst activity and α-olefin product distribution are explored.

Introduction

Current commercial processes for the production of linear α-olefins reflect both past and future market conditions. These conditions include relative growth rates of various α-olefin end uses, captive requirements of α-olefin producers, development of new end uses, feedstock cost considerations, product quality requirements, and catalyst limitations.[1−4] Because of these various concerns, full-range α-olefin production (e.g., production of $C_4-C_{20}+$ α-olefins) has raised a somewhat elevated barrier to entry, requiring major producers to balance the supply and demand of multiple products, each one having different end uses and values. For example, Chevron Phillips sells 13 different α-olefin fractions, as well as several derivatives! The advantage to full-range production is the ability to leverage temporarily undervalued products against those that are economically advantaged, thereby insulating the business from some of the vagaries of the petrochemical cycle.

An emerging alternative to full-range α-olefin production is the selective production of α-olefins. This has been done for many years commercially using IFP's Alphabutol process for dimerizing ethylene to 1-butene.[5,6] Typically, because 1-butene has had a historically low market value relative to ethylene, these dimerization facilities have been used to produce 1-butene for captive plant requirements in remote locations where butene is not readily available. A very interesting and more recent trend is the emergence of multiple catalyst systems for ethylene trimerization,[7−11] and even more recently, tetramerization, to selectively prepare 1-hexene and 1-octene.[12−17] Chevron Phillips was the first commercial

*To whom correspondence should be addressed. E-mail: smallbl@cpchem.com. Phone: 281-359-0281.

(1) Lappin, G. R.; Sauer, J. D., Eds. *Alpha Olefins Applications Handbook*; Marcel Dekker, Inc.: New York, 1989.
(2) Vogt, D. In *Applied Homogeneous Catalysis with Organometallic Compounds*, 2nd ed.; Cornils, B.; Herrmann, W. H., Eds.; Wiley-VCH: Weinheim, 2002; p 240.
(3) Reuben, B.; Wittcoff, H. *J. Chem. Educ.* **1988**, *65* (7), 605.
(4) Kirschner, M. *ICIS Chem. Bus.* **2008**, April 21−27, 42.
(5) Olivier-Bourbigou, H.; Saussine, L. In *Applied Homogeneous Catalysis with Organometallic Compounds*, 2nd ed.; Cornils, B.; Herrmann, W. H., Eds.; Wiley-VCH: Weinheim, 2002; p 259.
(6) Al-Jarallah, A. M.; Anabtawi, J. A.; Siddiqui, M. A. B.; Aitani, A. M. *Catal. Today* **1992**, *14*, 1.
(7) Dixon, J. T.; Green, M. J.; Hess, F. M.; Morgan, D. H. *J. Organomet. Chem.* **2004**, *689*, 3641.
(8) McGuinness, D. S.; Brown, D. B.; Tooze, R. P.; Hess, F. M.; Dixon, J. T.; Slawin, A. M. Z. *Organometallics* **2006**, 3605.
(9) Wu, F.-J. (BP Amoco) U.S. Patent 5968866,1999.
(10) Carter, A.; Cohen, S. A.; Cooley, N. A.; Murphy, A.; Scutt, J.; Wass, D. F. *Chem. Commun.* **2002**, 858.
(11) McConville, D. H.; Ackerman, L.; Li, R. T.; Bei, X.; Kuchta, M. C.; Boussie, T.; Walzer, J. F.; Diamond, G.; Rix, F. C.; Hall, K. A.; LaPointe, A.; Longmire, J.; Murphy, V.; Sun, P.; Verdugo, D.; Schofer, S.; Dias, E. (ExxonMobil) U.S. Patent 7414006 2008.
(12) Bollmann, A.; Blann, K.; Dixon, J. T.; Hess, F. M.; Killian, E.; Maumela, H.; McGuinness, D. S.; Morgan, D. H.; Neveling, A.; Otto, S.; Overett, M.; Slawin, A. M. Z.; Wasserscheid, P.; Kuhlmann, S. *J. Am. Chem. Soc.* **2004**, 14712.
(13) Overett, M. J.; Blann, K.; Bollmann, A.; Dixon, J. T.; Haasbroek, D.; Killian, E.; Maumela, H.; McGuinness, D. S.; Morgan, D. H. *J. Am. Chem. Soc.* **2005**, 10723.
(14) Overett, M. J.; Blann, K.; Bollmann, A.; Dixon, J. T.; Hess, F.; Killian, E.; Maumela, H.; Morgan, D. H.; Neveling, A.; Otto, S. *Chem. Commun.* **2005**, 622.
(15) Wass, D. F. *Dalton Trans.* **2007**, 816.
(16) Blann, K.; Bollmann, A.; Dixon, J. T.; Neveling, A.; Morgan, D. H.; Maumela, H.; Killian, E.; Hess, F. M.; Otto, S.; Pepler, L.; Mahomed, H. A.; Overett, M. J.; Green, M. J. (Sasol) U.S. Patent 7297832, 2007.
(17) Blann, K.; Bollmann, A.; Dixon, J. T.; Neveling, A.; Morgan, D. H.; Maumela, H.; Killian, E.; Hess, F. M.; Otto, S.; Pepler, L.; Mahomed, H. A.; Overett, M. J.; Green, M. J. (Sasol) WO 2004/056479 A1, 2007.

Published on Web 11/19/2010

Scheme 1

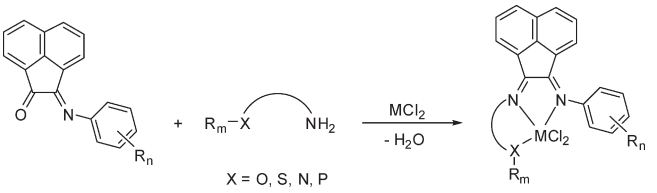

producer of selective 1-hexene,[18] and other companies have since followed.[19] While selective α-olefin production can meet the growing needs of polyethylene comonomer end users, the attractiveness of making a single α-olefin fraction must be balanced with the risk of "commoditization" or downturns in demand. In addition to the commercial and emerging ethylene oligomerization technologies, the α-olefin industry is also affected by non-ethylene-based processes, such as the availability of refinery 1-butene,[20] Fischer−Tropsch α-olefins,[21] and butadiene-based 1-octene.[22,23]

Clearly, maintaining a portfolio of full-range and selective α-olefin options provides needed flexibility for large-scale producers. Recently, in addition to our selective oligomerization studies, we reported a new family of pendant donor modified α-diimine complexes for the oligomerization of ethylene.[24−27] The complexes were readily prepared via a selective 1:1 reaction of various anilines with acenaphthenequinone, followed by a template-mediated condensation of a primary aliphatic amine with the remaining ketone group (Scheme 1). Many of these complexes, following activation with MMAO, were highly active for the preparation of linear α-olefins. In particular, the NNS- and NNP-ligated systems made useful product distributions and exhibited high catalyst activities. In this report, further structural variations on the imino-aryl rings and the phosphine and thioether substituents have been introduced. These complexes have been screened for ethylene oligomerization activity; X-ray crystallographic

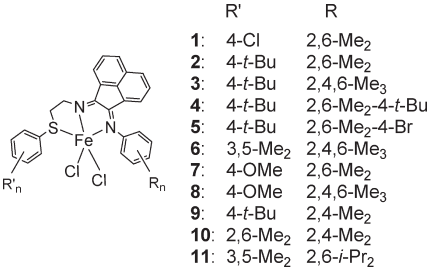

Figure 1. Schematic diagrams of iron(II) NNS complexes **1**−**11**.

Scheme 2

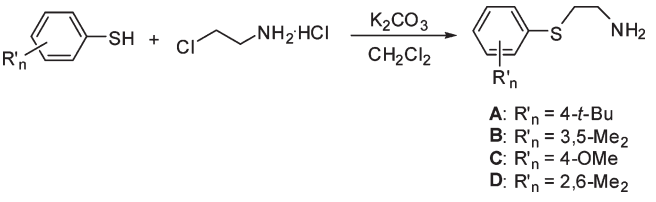

Scheme 3

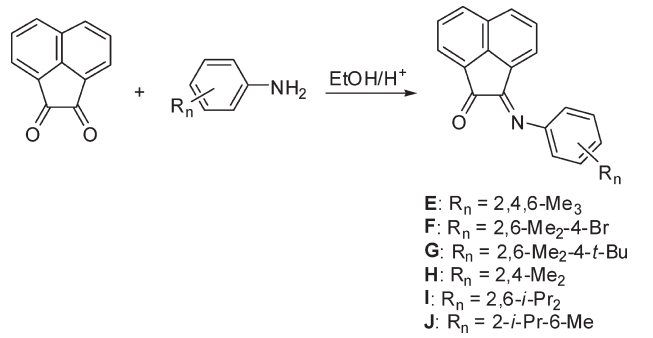

studies have been used to supplement the discussion of catalyst behavior.

Results and Discussion

Oligomerization Using NNS-Ligated Iron Complexes. Several new thioetheramines were prepared by the halide displacement method disclosed in the literature (Scheme 2).[24,28] These thioetheramines were used to prepare NNS-ligated iron complexes **1**−**11**, via addition to the appropriate acenaphthene-monoimines in the presence of $FeCl_2 \cdot 4H_2O$ or $FeCl_2$. The acenaphthene-monoimines were made according to Scheme 3. Complexes **1** and **11** were reported in our prior publication;[24] the thioether and imine substituents on complexes **2**−**10** were chosen to allow a systematic study of the steric and electronic effects of modifications to the NNS catalysts, especially with respect to the Schulz−Flory K values (K = mol C_{n+2}/mol C_n) and the catalyst activities. The schematic structures of complexes **1**−**11** are shown in Figure 1.

Oligomerization of ethylene was carried out for each of the complexes. The conditions and results of the experiments are reported in Table 1. More details are described in the Experimental Section. The first modification to the NNS systems was the replacement of the Cl in **1** with a *tert*-butyl group in complex **2**. Given the solid-state structure of

(18) CPChem's proprietary 1-hexene process is based on Cr-pyrrole complexes. Reagan, W. K.; Conroy, B. K. (Phillips) U.S. Patent 5198563, 1993. Bridges, S. D.; Abbott, R. G.; Baralt, E. J.; Knudsen, R. D.; Kreischer, B. E.; Small, B. L. (CPChem) U.S. Patent 7384886, 2008. Kreischer, B. E. (CPChem) U.S. Patent 7476775, 2009. Battiste, D. R. (CPChem) U.S. Patent 7396970, 2008. Freeman, J. W.; Ewert, W. M.; Kreischer, B. E.; Knudsen, R. D.; Cowan, G. D. (CPChem) U.S. Patent 6455648, 2002. Kreischer, B. E.; Ewert, W. M.; Knudsen, R. D. (CPChem) U.S. Patent 6380451, 2002. Conroy, B. K.; Pettijohn, T. M.; Reagan, W. K.; Freeman, J. W. (Phillips) U.S. Patent 5376612, 1994. Conroy, B. K.; Pettijohn, T. M.; Reagan, W. K.; Freeman, J. W. (Phillips) U.S. Patent 5523507, 1996.

(19) Recent press releases have indicated that other companies are intent on producing 1-hexene via selective ethylene trimerization.

(20) ExxonMobil and Texas Petrochemicals can produce 1-butene by distillation from raffinate streams.

(21) Sasol extracts α-olefins in the comonomer range by distilling them from Fischer−Tropsch hydrocarbon streams. Sasol has also employed successive hydroformylation, hydrogenation, and alcohol dehydration to convert the odd-carbon-number olefins to even-numbered comonomer olefins, i.e., 1-heptene into 1-octene.

(22) Dow has recently constructed a plant in Spain to prepare 1-octene from butadiene: Schaart, B. J.; Pelt, H. L.; Jacobsen, G. B. (Dow) U.S. Patent 5254782, 1993.

(23) Clement, N. D.; Routaboul, L.; Grotevendt, A.; Jackstell, R.; Beller, M. *Chem.—Eur. J.* **2008**, *14*, 7408.

(24) Schmiege, B. M.; Carney, M. J.; Small, B. L.; Gerlach, D. L.; Halfen, J. A. *Dalton Trans.* **2007**, 2547.

(25) Small, B. L.; Rios, R.; Fernandez, E. R.; Carney, M. J. *Organometallics* **2007**, *26*, 1744.

(26) Small, B. L.; Carney, M. J. (CPChem) U.S. Patent 7268096, 2007.

(27) Small, B. L.; Carney, M. J. (CPChem) U.S. Patent 7129304, 2006. Small, B. L.; Carney, M. J. (CPChem) U.S. Patent 7271121, 2007.

(28) Katritzky, A. R.; Hu, Y.-J.; He, H.-Y.; Mehta, S. *J. Org. Chem.* **2001**, *66*, 5590.

Table 1. Ethylene Oligomerization Data for NNS-Ligated Fe Catalysts[a]

entry	cat.	amt (mg)	MMAO Al:Fe	$P_{ethylene}$ (psig)	length (min)	T (°C)	T_{max} (°C)	yield C_4-C_{20} (g)	prod (g prod/ mmol cat)	K (C_{12}/C_{10})	C_6% purity	C_8% purity	C_{10}% purity
1	**1**	3.0	500	1000	60	50	68	110	21 400	0.65	99.5	99.3	99.0
2	**2**	1.0	300	1000	60	50	55	91.0	54 900	0.73	99.7	99.6	99.6
3	**3**	1.0	300	1000	60	50	58	149	91 600	0.72	99.8	99.7	99.5
4	**4**	1.2	300	1000	60	50	62	27.9	15 300	0.68	99.6	99.4	99.2
5	**5**	1.2	300	1000	60	50	53	57.9	32 900	0.72	99.4	99.3	99.2
6	**6**	1.2	300	1000	60	50	53	54.8	26 900	0.72	99.3	99.3	99.3
7	**7**	1.5	300	1000	30	50	65	98.1	39 400	0.72	99.7	99.7	99.6
8	**8**	1.2	300	1000	60	50	52	98.7	48 600	0.78	99.5	99.5	99.4
9	**9**	3.0	500	1000	30	50	50	~40	~20 100	0.24 - 0.61 C8 - 18			
10	**10**	3.0	300	1000	30	35	37	14.0	2700	0.74			
11	**11**	3.2	500	1000	60	50	50	116	35 500	0.85		98.9	

[a] All reactions were run in cyclohexane solvent.

unactivated **1** with an unbound thioether,[24] it was reasoned that an electron -donating alkyl group (in this case *tert*-butyl) might stabilize the active species. When tested under similar conditions to those for **1**, complex **2** showed higher productivity (entry 2). Replacing the 2,6-dimethylphenyl ring of **2** with a mesityl (2,4,6-trimethyl) group gave an even more active catalyst system, **3** (entry 3), but further pushing this trend with a *tert*-butyl group on the N-aryl *para* position gave the significantly less active **4** (entry 4). Using an electron-withdrawing group (Br) on the N-aryl ring increased the activity, placing complex **5** between **2** and **4** on the activity scale (entry 5). These significant activity differences between similar systems would tempt one to make sweeping arguments regarding ligand electronics and catalyst activity. In fact, computational studies have been performed on related pyridine bisimine (PBI) Fe catalysts,[29] with the contention that subtle changes in ligand electronics may dramatically affect catalyst activity. While this may be the case for these NNS (and NNP) catalysts, it is noted that only one set of conditions is being used. A batch activity, while somewhat useful, often does not give a good picture of catalyst lifetime, thermal stability, or productivity.

Further electronic modifications were tested in complexes **6**−**8**. Use of *meta*-methyl groups on the thioether aryl ring in **6** gave a system with lower activity than the *p*-*tert*-butyl catalysts **2** and **3**. Interestingly, it was also much easier to isolate **2**−**5** in higher yield (>73%) than **6** (<50%). Complexes **7** and **8**, with a *p*-methoxy group on the S-aryl rings, also produced highly active catalysts.

The productivities for complexes **2**−**8** were all reasonably high, with **3** giving the highest productivity of >90 000 g product/mmol Fe. The second area of interest was the Schulz−Flory K value and whether it could be modulated by these subtle electronic changes. From the data for **1**−**8**, with the possible exception of **8**, the K values were relatively constant, ranging between 0.65 (entry 4) and 0.73 (entry 5). While these K value changes would be considered significant in a commercial setting, they do not appear to represent any trend from these batch data. The only exception is complex **8**, with a K value of 0.78. Certainly the interaction of aluminum with the methoxy group could be proposed as a significant difference in this system; regardless of explanation, this high K value is moving to the high end of the typically relevant distributions.[1]

Further modifications to the NNS ligands were introduced in complexes **9** and **10**. In **9**, the steric bulk of the N-aryl group was reduced, resulting in a lighter distribution, in agreement

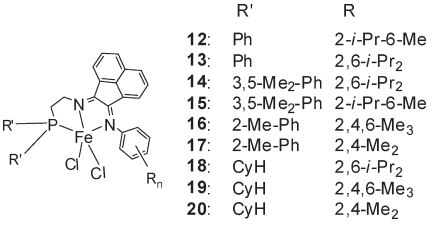

Figure 2. Schematic diagrams of iron(II) NNP complexes **12**−**20**.

with literature precedent.[25,30,31] Due to the loss of butene from the reactor prior to analysis, and a nonconstant K value, the productivity of this system could only be estimated. Even the mol C_{10}/mol C_8 ratio for this system was a remarkably low 0.24, indicating that the actual ratio of C_6/C_4 produced was much lower, essentially meaning that **9** is an ethylene dimerization catalyst. The higher olefins are likely produced by reincorporation, i.e., co-dimerization of higher olefins with ethylene. Thus, the broadening of the K value is conversion dependent, as was discussed for another system in our prior publication.[25] In complex **10**, the steric bulk was added to the S-aryl ring by placing methyl groups at the *ortho* positions. The K value did in fact increase, but with the effect of dramatically reducing catalyst activity. It is an interesting observation that *ortho* substituents on the pendant donor aryl rings tend to suppress catalyst activity much more than *ortho* groups on the N-aryl rings. This observation is further supported by the results for the previously reported complex **11**, with bulky 2,6-isopropyl substituents on the N-aryl ring. Despite this steric bulk, **11** is an order of magnitude more active than **10**. This trend holds true for the NNP catalysts as well (see following discussion).

Oligomerization Using NNP-Ligated Iron Complexes. Seven new NNP Fe complexes (Figure 2) were prepared using new 2-phosphinoethylamines. The complexes were made according to our previously reported method[24] by reaction of the phosphinoamine with the appropriate acenaphthene-based monoimine in *n*-butanol in the presence of $FeCl_2$. NNP-ligated iron(II) complexes **12** and **13** were disclosed earlier[24] and are included here for comparison purposes.

Oligomerization experiments for catalysts **12**−**20** are reported in Table 2. Similar to the NNS systems and for many other ethylene oligomerization systems, the product distributions

(29) Zhang, T.; Sun, W.-H.; Li, T.; Yang, X. *J. Mol. Catal. A: Chem.* **2004**, *218*, 119.

(30) Small, B. L.; Brookhart, M. *J. Am. Chem. Soc.* **1998**, *120*, 7143.

(31) Britovsek, G. J. P.; Mastroianni, S.; Solan, G. A.; Baugh, S. P. D.; Redshaw, C.; Gibson, V. C.; White, A. J. P.; Williams, D. J.; Elsegood, M. R. J. *Chem.—Eur. J.* **2000**, *6* (12), 2221.

Table 2. Ethylene Oligomerization Data for NNP-Ligated Fe Catalysts[a]

entry	cat.	amt (mg)	MMAO Al:Fe ratio	$P_{ethylene}$ (psig)	length (min)	T (°C)	T_{max} (°C)	yield (g)	prod (g prod/ mmol cat)	K (C_{12}/C_{10})	C_6% purity	C_8% purity	C_{10}% purity
12	**12**	3.1	500	1000	60	50	63	108	35 200	0.49−0.61	99.4	99.1	
13	**13**	1.8	300	1000	90	50	52	124	70 600	0.60	99.4	99.3	
14	**14**	3.0	250	1000	60	50	54	48.7	11 900	0.72			
15	**15**	1.9	350	1000	60	50	53	149	55 600	0.60	99.6	99.5	99.4
16	**16**	3.0	300	1000	30	42	42	8.9	1970	0.82			
17	**17**	3.0	500	1000	30	34	34	∼10, n.d.		mostly C_4			
18	**18**	2.0	500	1000	30	45	45	4.4	1520	0.88			
19	**19**	2.0	500	1000	30	50	55	22.5	7300	0.86			
20	**20**	2.0	500	1000	30	50	65	∼50	15 900	mostly C_4	99.8	99.3	98.9

[a] All reactions were run in cyclohexane solvent.

are clearly tied to the ligand steric environment. Complexes **12** and **13** illustrate this trend, as moving from a CH_3 group to an *i*-Pr group at the 6-position of the N-aryl ring causes a significant increase in the *K* value (entries 12 and 13). Complex **14** introduces an additional steric consideration, with methyl groups at *meta* positions on the P-aryl rings. This change led to a significant increase in the *K* value from about 0.60 to 0.72 (entries 13 and 14), indicative of a *meta* steric influence. This 3,5-dimethyl effect has been cited in the literature for other phosphine systems[32,33] and is likely due to a more rigidly enforced ring conformation induced by the *meta* methyl groups. The ligand bulkiness was decreased in complex **15** (entry 15) by changing one of the *i*-Pr groups on the imine aryl ring to a CH_3 group, and a corresponding decrease in *K* value to 0.60 was observed (entry 15). A similar steric trend is observed for **12** and **13**. It is also interesting to note that catalysts **13** and **15** behave similarly, both with respect to catalyst activity and product distribution, indicating that the 3,5-dimethyl effect can be almost directly offset by steric tuning on the imine aryl ring.

Thus, steric tuning of the P-aryl *meta* positions provided a means for modulating the product distribution without significantly affecting the catalyst activity. However, addition of an *ortho*-methyl group on the P-aryl ring caused a dramatic reduction in activity. For example, the *o*-tolyl phosphines of complexes **16** and **17** (entries 16 and 17) produced only modestly active catalysts, similar to NNS system **10**. Similarly, complexes containing bulky cyclohexyl phosphine substituents (complexes **18** and **19**) displayed low catalyst productivity as well as the expected shift of product distribution toward higher *K* values (K = 0.86−0.88). Furthermore, complexes **17** and **20** demonstrate that while removal of steric bulk at the imine nitrogen can improve catalyst productivity, it also causes a dramatic shift in catalyst performance from oligomerization to ethylene dimerization.

Product distribution data for catalysts **12**−**20** demonstrates the ability to adjust the *K* value by changing the steric environment surrounding either the phosphine or the imine nitrogen. Catalyst activity data for these same complexes suggests that activity is more severely impacted by modifications made to the phosphine substituents. Crystallographic studies on selected iron(II) complexes supported by NNS and NNP ligands were carried out to better understand the details of metal−ligand binding and to examine possible connections between solid-state structure and catalyst performance.

Crystallographic Studies. Iron(II) Complexes Supported by Tridentate NNS Ligands. Crystals of NNS-ligated complexes **2** and **4** were grown by pentane diffusion into a concentrated dichloromethane solution of each complex, which resulted in dichloromethane incorporation into each unit cell. Noncoordinating dichloromethane was chosen as the crystallization solvent to avoid solvent coordination to the iron center and, instead, to promote ligation of the thioether sulfur atom. X-ray data collection parameters for **2** and **4** are contained in Table 3, while the molecular structures of **2** and **4** are shown in Figures 3 and 4, respectively. Selected distances and angles are provided in Table 4. The crystal structure of a thioether ligated complex **11** was reported by us previously;[24] distance and angle data for **11** are listed in Table 4 for comparison purposes. In our previous study, we found that sulfur ligation to Fe was dependent on the thioether aryl substituents. For example, the thioether sulfur atom in *para*-Cl complex **1** did not coordinate to the iron center (a chloride-bridged dimer was formed instead),[24] whereas the sulfur did bind in 3,5-dimethyl derivative **11**, albeit with a relatively long Fe−S distance (2.7126 Å).[24] In the present study, the structures of **2** and **4** clearly show sulfur ligation to form monomeric, five-coordinate complexes. Similar to **11**, the Fe−S bond distances in **2** and **4** are long, with the Fe−S distance in **4** (2.8170 Å) being the longest distance among our family of iron(II) complexes and one of the longest Fe−S distances yet observed.[24] Further inspection of Table 4 shows that, in contrast to **11**, complexes **2** (both independent molecules) and **4** display relatively dissimilar Fe−N(1) and Fe−N(2) distances, with the Fe−N(1) (imine) bond being significantly shorter than the Fe−N(2) (imine) bond. These dissimilar Fe−N bond lengths are observed for both independent molecules of complex **2** (Fe−N(3) < Fe−N(4) for molecule 2 of **2**). These Fe−N distances are much more similar in **11**. Furthermore, complexes **2** and **4** exhibit larger (more linear) N(2)−Fe−S angles (ranging from 152.70° to 156.24°) and larger Cl(1)−Fe−Cl(2) angles than **11**. Due to these large angles, **2** and **4** are perhaps best characterized as distorted trigonal-bipyramidal structures, with the sulfur and imino-aryl nitrogen atoms occupying apical positions.

It is also notable that for **2** the Fe−S bond lengths and the N−Fe−S angles are slightly different in the two independent molecules. Close inspection of the packing diagram for **2** indicates that the differences are not due to obvious intermolecular interactions. However, we note that the Fe−S bonding is quite long (weak), and weak solid-state effects could alter the Fe−S bond length by ±0.05 Å, with a corresponding small impact on the N−Fe−S angles.

Unfortunately, catalyst activity (Table 1) does not clearly correlate with the Fe−S bond length or with other structural parameters in Table 4. Complex **4** displays relatively low

(32) Trabesinger, G.; Albinati, A.; Feiken, N.; Kunz, R.; Pregosin, P. S.; Tschoerner, M. *J. Am. Chem. Soc.* **1997**, *119*, 6315.
(33) Dotta, P.; Kumar, P. G. A.; Pregosin, P. S. *Organometallics* **2004**, *23*, 2295.

Table 3. Summary of X-ray Crystallographic Data for Iron(II) Complexes 2, 4, 14, and 18[a]

	2·1.25CH_2Cl_2	**4**·CH_2Cl_2	**14**·C_2H_3N	2 **18**·C_2H_3N
empirical formula	$C_{33.25}H_{34.50}Cl_{4.50}FeN_2S$	$C_{37}H_{42}Cl_4FeN_2S$	$C_{44}H_{48}Cl_2FeN_3P$	$C_{78}H_{101}Cl_4Fe_2N_5P_2$
fw	709.56	744.44	776.57	1424.08
temperature (K)	173(2)	173(2)	173(2)	173(2)
cryst syst	triclinic	monoclinic	monoclinic	triclinic
space group	$P\bar{1}$	$C2/c$	$I2/a$	$P2_1/n$
a (Å)	14.780(3)	30.520(6)	22.288(2)	15.583(2)
b (Å)	14.781(3)	14.238(2)	12.3291(13)	14.318(2)
c (Å)	16.780(4)	18.924(4)	29.903(3)	33.016(5)
α (deg)	87.90(2)	90	90	90
β (deg)	66.23(2)	116.20(3)	93.632(1)	91.984(2)
γ (deg)	85.14(1)	90	90	90
V (Å^3)	3342.8(12)	7378(2)	8200.5(15)	7361.9(19)
Z	4	8	8	4
d_{calcd} (Mg·m^{-3})	1.410	1.340	1.258	1.285
cryst size (mm)	0.44 × 0.20 × 0.12	0.45 × 0.32 × 0.06	0.35 × 0.25 × 0.15	0.40 × 0.40 × 0.30
abs coeff (mm^{-1})	0.90	0.78	0.571	0.629
$2\theta_{max}$ (deg)	50.02	52.06	54.98	50.06
transmn range	0.6930−0.8997	0.8258−1.0	0.8252−0.9193	0.7871−0.8338
no. of reflns collected	10 205	7388	39 853	79 366
no. of indep reflns	9704	7249	9318	12 995
no. of obsd reflns	6557	4406	7255	9990
no. of variables	757	420	497	829
R_1 (wR_2)[b] [$I > 2\sigma(I)$]	0.0681 (0.1642)	0.0718 (0.1693)	0.0380 (0.0914)	0.0554 (0.1308)
goodness-of-fit (F^2)	1.021	1.011	1.054	1.107
diff peaks (e$^-$·Å^{-3})	1.07, −1.05	1.06, −0.71	0.746, −0.306	0.979, −0.549

[a] See Experimental Section for additional data collection, reduction, and structure solution and refinement details. [b] $R_1 = \sum||F_o| - |F_c||/\sum|F_o|$; $wR_2 = [\sum[w(F_o^2 - F_c^2)^2]]^{1/2}$ where $w = 1/\sigma^2(F_o^2) + (aP)^2 + bP$.

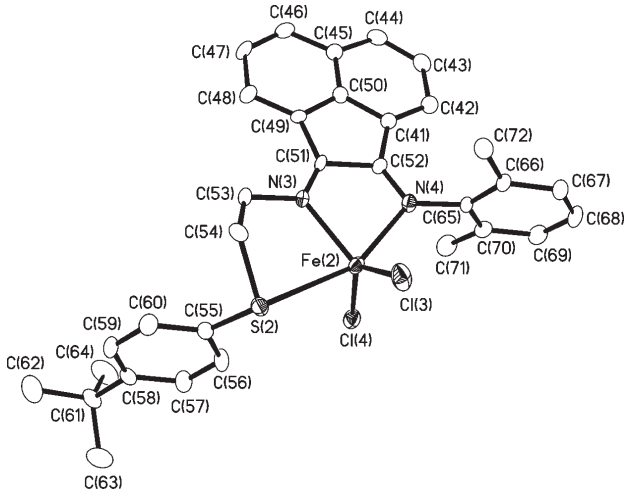

Figure 3. Thermal ellipsoid representation (35% probability boundaries) of the X-ray crystal structure of **2** (molecule 2) with hydrogen atoms omitted for clarity.

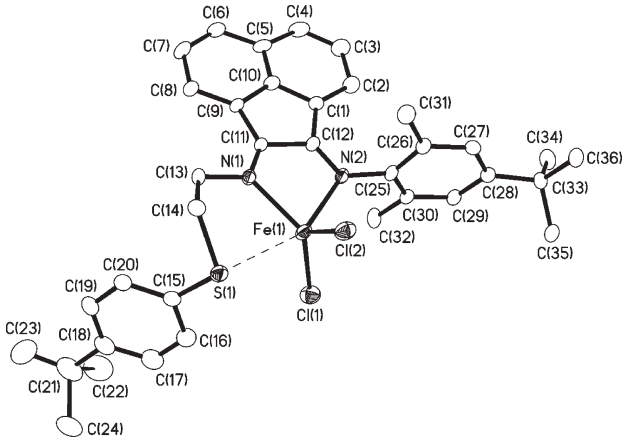

Figure 4. Thermal ellipsoid representation (35% probability boundaries) of the X-ray crystal structure of **4** with hydrogen atoms omitted for clarity.

productivity and possesses a long Fe−S bond. Furthermore, **10** has low productivity and, although not structurally characterized, should display (at best) weak Fe−S binding due to the 2,6-dimethyl substituents on the S-aryl ring. However, complex **1**, in which the sulfur is not coordinated to iron (at least not in the solid state), displays higher activity than complex **4**. Thus clear and convincing correlations between the structure and catalyst performance are not readily apparent.

Iron(II) Complexes Supported by Tridentate NNP Ligands. Crystals of NNP-ligated complexes **14** and **18** were grown by slow cooling of saturated acetonitrile solutions of each compound, which resulted in acetonitrile incorporation into each unit cell. In contrast to sulfur-containing complexes, phosphorus effectively competes with donor solvents such as acetonitrile for coordination to the iron center. The structures of **14** and **18** are shown in Figures 5 and 6, respectively; selected distances and angles can be found in Table 5. The crystal structure for **13** was reported previously;[24] distance and angle data for **13** are included in Table 3 for comparison. As with **13**, and in contrast to the NNS-ligated complexes **2** and **4**, the five-coordinate geometries of **14** and **18** are best described as distorted square pyramidal; the tridentate ligand and one chloride ligand form the pyramidal base and the remaining chloride resides in the apical position. As shown in Table 5, the Fe−N and Fe−Cl distances, as well as N−Fe−N, N−Fe−P, and Cl−Fe−Cl angles, are similar among the three NNP complexes. The Fe−P distances (2.5455 Å for **14** and 2.5377 and 2.5414 Å for **18**) are 0.041 to 0.048 Å longer than that previously found for **13**, but remain in the range of Fe−P bond lengths typical of five-coordinate, high-spin Fe(II) centers.[24] The longer Fe−P

Table 4. Selected Distances (Å) and Angles (deg) for NNS-Ligated Metal Complexes

	2			**4**		**11**	
molecule 1		molecule 2					
Fe(1)−N(1)	2.102(5)	Fe(2)−N(3)	2.094(5)	Fe(1)−N(1)	2.112(4)	Fe(1)−N(1)	2.136(2)
Fe(1)−N(2)	2.245(5)	Fe(2)−N(4)	2.244(4)	Fe(1)−N(2)	2.227(4)	Fe(1)−N(2)	2.165(3)
Fe(1)−S(1)	2.6980(19)	Fe(2)−S(2)	2.7483(18)	Fe(1)−S(1)	2.8170(17)	Fe(1)−S(1)	2.7126(10)
Fe(1)−Cl(1)	2.241(2)	Fe(2)−Cl(3)	2.252(2)	Fe(1)−Cl(1)	2.2560(16)	Fe(1)−Cl(1)	2.2665(10)
Fe(1)−Cl(2)	2.2822(18)	Fe(2)−Cl(4)	2.277(2)	Fe(1)−Cl(2)	2.2676(16)	Fe(1)−Cl(2)	2.3089(10)
N(1)−Fe(1)−N(2)	77.2(2)	N(3)−Fe(2)−N(4)	77.79(18)	N(1)−Fe(1)−N(2)	78.03(14)	N(1)−Fe(1)−N(2)	77.81(9)
N(1)−Fe(1)−S(1)	75.88(17)	N(3)−Fe(2)−S(2)	78.78(13)	N(1)−Fe(1)−S(1)	76.65(11)	N(1)−Fe(1)−S(1)	75.24(7)
N(2)−Fe(1)−S(1)	152.70(13)	N(4)−Fe(2)−S(2)	156.24(13)	N(2)−Fe(1)−S(1)	154.66(11)	N(2)−Fe(1)−S(1)	144.24(7)
Cl(1)−Fe(1)−Cl(2)	129.26(8)	Cl(3)−Fe(2)−Cl(4)	131.32(8)	Cl(1)−Fe(1)−Cl(2)	126.45(6)	Cl(1)−Fe(1)−Cl(2)	116.96(4)

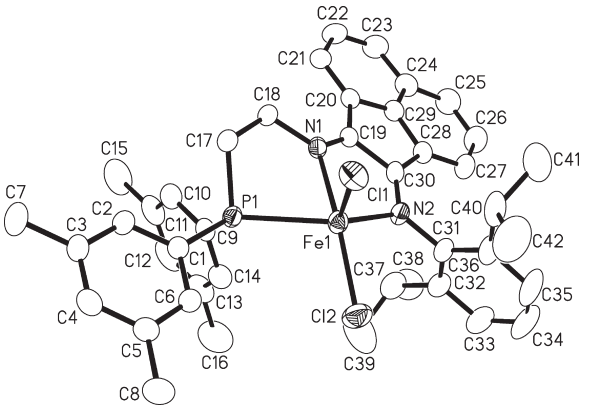

Figure 5. Thermal ellipsoid representation (35% probability boundaries) of the X-ray crystal structure of **14** with hydrogen atoms omitted for clarity.

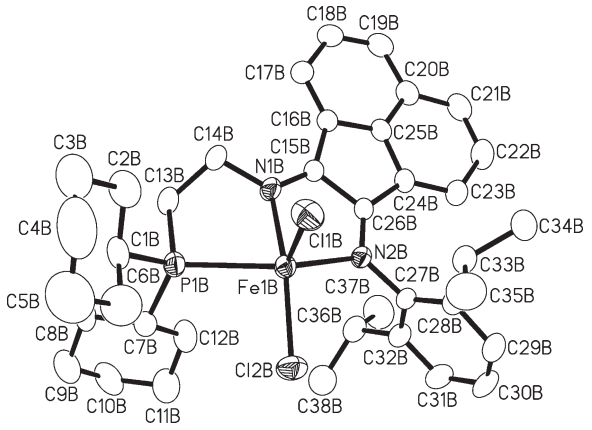

Figure 6. Thermal ellipsoid representation (35% probability boundaries) of the X-ray crystal structure of **18** with hydrogen atoms omitted for clarity.

length in **18** (relative to **13**) may be ascribed to the greater steric bulk of dicyclohexylphosphine relative to diphenylphosphine. The longer Fe−P bond in **14** (relative to **13**) is perhaps a manifestation of the steric influence of the *meta* methyl groups on P-aryl conformations, as mentioned previously. In both cases, the slight elongation of the Fe−P distance is consistent with a modest increase in steric bulk at phosphorus, and, as noted previously, increased steric bulk at phosphorus correlates with the higher K values found for **14** ($K = 0.72$) and **18** ($K = 0.88$) relative to the less sterically congested **13** ($K = 0.60$).

Conclusion

A variety of phosphinoamines, thioetheramines, and anilines have been used to illustrate the structural diversity available in pendant donor modified α-diimine complexes. Steric and electronic modifications have been used to show how this diversity can affect catalyst activity and ethylene oligomer distributions. It is likely that continued study of this new family of ligands will open the door to other catalytic transformations as the coordination and synthetic chemistries are better understood and applied.

Experimental Section

Materials and Methods. Heptane and cyclohexane were purchased from Aldrich or acquired from internal company resources, degassed, and pumped repeatedly in a circular loop over a molecular sieve bed. Monoimines **I** and **J** were reported in our prior publication.[24] MMAO-3A (Al 7% by wt) was purchased from Akzo Nobel. All of the 2-phosphinoethylamines were purchased from Digital Specialty Chemicals. All other starting materials were purchased from Aldrich and used as received.

Product Analysis. A Hewlett-Packard 6890 Series GC system with an HP-5 50 m column with a 0.2 mm inner diameter was used for α-olefin characterization. An initial temperature of 35 °C and a rate of 2.4 °C/min were used to raise the temperature to 52 °C, followed by a rate of 15.0 °C/min to raise the temperature to 157 °C. A final ramp rate of 22.5 °C/min was used to reach the final temperature of 250 °C. ChemStation from Hewlett-Packard was used to analyze the collected data. Odd-carbon-numbered, nonvolatile internal standards were used to estimate catalyst productivity. Volatile α-olefin (i.e., 1-hexene and 1-butene) amounts were estimated by extrapolation using the Schulz−Flory K values.

Ethylene Oligomerization/Polymerization. A 500 mL Zipperclave reactor from Autoclave Engineers was used for the oligomerization and polymerization reactions. The catalyst was dissolved in a small amount of dichloromethane in an NMR tube, which was then sealed and bound to the stirrer shaft of the clean, dry reactor. The reactor was evacuated, then charged with cyclohexane (typically 200 mL) and the aluminum cocatalyst/scavenger. The desired pressure of ethylene was introduced, and the reactor stirrer was started, resulting in breakage of the NMR tube and catalyst activation. Ethylene was fed "on demand" using a TESCOM regulator, and the reactor temperature was maintained by internal cooling. Reactions were terminated by slowly venting the reactor over a few minutes.

Preparation of Thioetheramines A −D. 2-(4-*tert*-Butylphenylthio)ethylamine (A). To a stirring mixture of 4.36 g (38.0 mmol) of 2-chloroethylamine hydrochloride and 12.00 g (87.0 mmol) of K_2CO_3 in 30 mL of $CHCl_3$ was added 4.82 g (29.0 mmol) of 4-*tert*-butylbenzenethiol. The mixture was stirred at 50 °C in a sealed vial overnight. The mixture was washed three times with distilled water, dried with $MgSO_4$, and filtered. Volatiles were removed in vacuo, leaving 4.50 g (74%) of clear oil. ^{1}H NMR (300 MHz, $CDCl_3$): δ 7.32, m, 4H; 2.93, m, 4H; 1.42, br s, 2H; 1.30, s, 9H.

2-(3,5-Dimethylphenylthio)ethylamine (B). To a stirring mixture of 1.93 g (9.4 mmol) of 2-bromoethylamine hydrobromide and 3.00 g (21.7 mmol) of K_2CO_3 in 30 mL of CH_2Cl_2 was added

Table 5. Selected Distances (Å) and Angles (deg) for NNP-Ligated Metal Complexes

13		14		18			
				molecule 1		molecule 2	
Fe(1)−N(1)	2.181(6)	Fe(1)−N(1)	2.1834(16)	Fe(1a)−N(1a)	2.196(3)	Fe(1b)−N(1b)	2.162(3)
Fe(1)−N(2)	2.166(6)	Fe(1)−N(2)	2.1750(16)	Fe(1a)−N(2a)	2.168(3)	Fe(1b)−N(2b)	2.190(3)
Fe(1)−P(1)	2.497(2)	Fe(1)−P(1)	2.5455(6)	Fe(1a)−P(1a)	2.5377(13)	Fe(1b)−P(1b)	2.5414(11)
Fe(1)−Cl(1)	2.287(2)	Fe(1)−Cl(1)	2.2958(6)	Fe(1a)−Cl(1a)	2.3192(12)	Fe(1b)−Cl(1b)	2.3112(12)
Fe(1)−Cl(2)	2.3131(18)	Fe(1)−Cl(2)	2.2846(6)	Fe(1a)−Cl(2a)	2.2799(12)	Fe(1b)−Cl(2b)	2.2847(11)
N(1)−Fe(1)−N(2)	75.9(2)	N(1)−Fe(1)−N(2)	74.98(6)	N(1a)−Fe(1a)−N(2a)	75.39(11)	N(1b)−Fe(1b)−N(2b)	75.20(11)
N(1)−Fe(1)−P(1)	74.01(16)	N(1)−Fe(1)−P(1)	73.09(4)	N(1a)−Fe(1a)−P(1a)	75.46(9)	N(1b)−Fe(1b)−P(1b)	76.67(8)
N(2)−Fe(1)−P(1)	135.20(16)	N(2)−Fe(1)−P(1)	132.67(4)	N(2a)−Fe(1a)−P(1a)	138.57(9)	N(2b)−Fe(1b)−P(1b)	138.23(8)
Cl(1)−Fe(1)−Cl(2)	111.98(8)	Cl(1)−Fe(1)−Cl(2)	106.28(2)	Cl(1a)−Fe(1a)−Cl(2a)	112.15(5)	Cl(1b)−Fe(1b)−Cl(2b)	112.30(5)

1.00 g (7.2 mmol) of 3,5-dimethylbenzenethiol. The mixture was stirred at room temperature under argon for two days. The mixture was washed twice with distilled water, dried with $MgSO_4$, and filtered. Volatiles were removed in vacuo, leaving a slightly cloudy yellow oil. Distillation of the oil under reduced pressure (0.10 Torr) at 80−95 °C produced 0.547 g (41.7%) of a clear liquid, which was identified as the desired product by its ^1H and ^{13}C NMR spectra. ^1H NMR (400 MHz, $CDCl_3$): δ 6.98, s, 2H; 6.82, s, 1H; 2.98, t, 2H; 2.89, t, 2H; 2.27, s, 6H; 1.55, br s, 2H. $^{13}C\{^1H\}$ NMR (100 MHz, $CDCl_3$): δ 138.58, 135.10, 128.21, 127.50, 41.00, 38.07, 21.29. EI mass spectrum: m/z 181 [M^+].

2-(4-Methoxyphenylthio)ethylamine (C). To a stirring mixture of 4.36 g (38.0 mmol) of 2-chloroethylamine hydrochloride and 12.00 g (87.0 mmol) of K_2CO_3 in 30 mL of $CHCl_3$ was added 4.07 g (29.0 mmol) of 4-methoxythiophenol. The mixture was stirred at 50 °C in a sealed vial overnight. The mixture was washed three times with distilled water, dried with $MgSO_4$, and filtered. Volatiles were removed in vacuo, leaving 4.97 g (89%) of yellow oil. ^1H NMR (300 MHz, $CDCl_3$): δ 7.36, d, 2H; 6.82, d, 2H; 3.80, s, O*Me*; 2.93, m, 4H; 1.42, br s, 2H.

2-(2,6-Dimethylphenylthio)ethylamine (D). To a stirring mixture of 2.73 g (23.6 mmol) of 2-chloroethylamine hydrochloride and 7.50 g (54.0 mmol) of K_2CO_3 in 20 mL of $CHCl_3$ was added 2.50 g (18.0 mmol) of 2,6-dimethylthiophenol. The mixture was stirred at 50 °C in a sealed vial overnight. The mixture was washed three times with distilled water, dried with Na_2SO_4, and filtered. Volatiles were removed in vacuo, leaving 2.83 g (86%) of a brown, oily solid. ^1H NMR (300 MHz, $CDCl_3$): δ 7.10, m, 3H; 2.80, d, 2H; 2.55, s, 6H; 1.42, br s, N*H*$_2$. Residual thiophenol appeared to also be present in about 10% by mass.

Preparation of Acenaphthene-monoimines E−H. Monoimine E. An ethanol (200 mL) suspension of acenaphthenequinone (10.0 g, 54.9 mmol) was treated with 1 mL of formic acid and heated to 70 °C, followed by slow, dropwise addition (over approximately 12 h) of a solution of 2,4,6-trimethylaniline (6.68 g, 49.5 mmol) in 100 mL of ethanol. The resulting mixture was stirred at 70 °C overnight, cooled, and filtered. Two crops of orange crystals were collected from the filtrate, upon cooling to 0 °C, for a total yield of 9.64 g (65%). ^1H NMR (300 MHz, $CDCl_3$): δ 8.18, d, 2H (chemical shift equivalence); 7.99, d, 1H; 7.81, t, 1H; 7.43, t, 1H; 6.95, s, 2H; 6.78, d, 1H, 2.37, s, 3H; 2.01, s, 6H.

Monoimine F. An ethanol (200 mL) suspension of acenaphthenequinone (5.00 g, 27.5 mmol) was treated with 2 mL of formic acid and heated to 75 °C, followed by slow, dropwise addition (over approximately 16 h) of a solution of 2,6-dimethyl-4-bromoaniline (5.49 g, 27.5 mmol) in 100 mL of ethanol. The resulting mixture was stirred and cooled to 25 °C and filtered to give about 100 mg of a brown powder. Cooling the filtrate to −30 °C for 1 h, followed by filtration, gave 153 mg of orange crystals, which were identified as the product with significant acenaphthenequinone present. A second crop collected after overnight crystallization at −30 °C gave 3.01 g (30%) of the desired product in 92% purity by mass. The remainder was identified as acenaphthenequinone. ^1H NMR (300 MHz, $CDCl_3$): δ 8.20, d, 1H; 8.18, d, 1H; 8.04, d, 1H; 7.83, t, 1H; 7.48, t, 1H; 7.30, s, 2H; 6.83, d, 1H; 2.02, s, 6H.

Monoimine G. An ethanol (150 mL) suspension of acenaphthenequinone (3.82 g, 21.0 mmol) was treated with 0.6 mL of formic acid and heated to 68 °C, followed by slow, dropwise addition (over approximately 24 h) of a solution of 2,6-dimethyl-4-*tert*-butylaniline (3.54 g, 20.0 mmol) in 160 mL of ethanol. The resulting mixture was stirred at 68 °C overnight, cooled, and filtered. Orange crystals were collected from the filtrate, upon cooling to 0 °C, for a yield of 1.64 g (24%). ^1H NMR (300 MHz, $CDCl_3$): δ 8.18, d, 2H (chemical shift equivalence); 7.99, d, 1H; 7.81, t, 1H; 7.43, t, 1H; 7.14, s, 2H; 6.70, d, 1H, 2.03, s, 6H; 1.38, s, 9H.

Monoimine H. An ethanol (200 mL) suspension of acenaphthenequinone (10.0 g, 54.9 mmol) was treated with 1 mL of formic acid and heated to 60 °C, followed by slow, dropwise addition (over approximately 12 h) of a solution of 2,4-dimethylaniline (5.40 mL, 44.0 mmol) in 100 mL of ethanol. The resulting mixture was stirred at 60 °C overnight, cooled, and filtered. Two crops of orange crystals were collected from the filtrate, upon cooling to 0 °C, for a total yield of 7.83 g (62%). ^1H NMR (300 MHz, $CDCl_3$): δ 8.18, m, 2H; 7.99, d, 1H; 7.80, t, 1H; 7.43, t, 1H; 7.13, s, 1H; 7.06, d, 1H, 6.92, d, 1H; 6.78, d, 1H; 2.39, d, 3H; 2.12, d, 3H.

Preparation of 2,6-Dimethyl-4-*tert*-butylaniline. 1-Nitro-4-*tert*-butyl-2,6-dimethylbenzene. 1-*tert*-Butyl-3,5-dimethylbenzene (40.0 g, 250 mmol) was dissolved in 60 mL of acetic acid. To this stirring mixture was added dropwise over 20 min 45 mL of a 50:50 v/v mixture of concentrated nitric and sulfuric acid, resulting in a temperature increase from 25 to 45 °C. Once the reaction had cooled to 30 °C, it was poured into water, ether was added, and the aqueous layer was extracted three times with ether. The ether layer was then extracted three times with a 1.0 M KOH solution. Removal of the ether left an oil that solidified upon standing. Pentane was added, and multiple crops of the desired product were collected as white needles from the resultant solution, for a total isolated yield of 18.5 g (36%). ^1H NMR (300 MHz, $CDCl_3$): δ 7.08, s, 2H; 2.30, s, 6H; 1.28, s, 9H.

2,6-Dimethyl-4-*tert*-butylaniline. 1-Nitro-4-*tert*-butyl-2,6-dimethylbenzene (12.0 g, 58.0 mmol) was dissolved in 160 mL of ethanol, followed by the addition of 20 mL of water. Then 4.8 g (43.2 mmol) of $CaCl_2$ dissolved in 20 mL of water was added to the stirring solution, followed by the addition of 50.0 g (76.5 mmol) of zinc powder.[34] The reaction was stirred overnight at 65 °C, then cooled to ambient temperature and filtered. The filtrate was extracted three times with ether, and the organic layer was dried over $MgSO_4$. Removal of the solvent gave 9.58 g (93%) of a brown oil. ^1H NMR (300 MHz, $CDCl_3$): δ 6.90, s, 2H; 3.40, br s, 2H; 2.11, s, 6H, 1.21, s, 9H.

Selected Syntheses for NNS-Ligated Iron Complexes. Complex 3. A solution of 0.250 g (1.20 mmol) of 2-(4-*tert*-butylphenylthio)-ethylamine **A** in 10 mL of cyclohexane was added to a mixture of 0.289 g (1.00 mmol) of monoimine **E** and 0.190 g (0.95 mmol) of $FeCl_2 \cdot 4H_2O$ in a 20 mL vial. The vial was sealed, and the contents were stirred overnight under nitrogen at 55 °C. The green product was isolated by filtration, washed with pentane, and dried to give 0.508 g (86%) of product. The compound analyzed as the monohydrate.

(34) Kuhn, W. E. *Organic Syntheses*; Wiley: New York, 1943; Coll. Vol. *2*, p 447.

Complex 4. A solution of 0.184 g (0.88 mmol) of 2-(4-*tert*-butylphenylthio)ethylamine **A** in 7 mL of cyclohexane was added to a mixture of 0.273 g (0.80 mmol) of monoimine **G** and 0.151 g (0.76 mmol) of $FeCl_2 \cdot 4H_2O$ in a 20 mL vial. The vial was sealed, and the contents were stirred overnight under nitrogen at 55 °C. The green product was isolated by filtration, washed with pentane, and dried to give 0.399 g (80%) of product. The compound analyzed as the monohydrate.

Complex 5. A solution of 0.214 g (1.02 mmol) of 2-(4-*tert*-butylphenylthio)ethylamine **A** in 3.5 mL of anhydrous *n*-butanol was added to a mixture of 0.400 g (1.10 mmol) of monoimine **F** and 0.127 g (1.00 mmol) of $FeCl_2$ in a 10 mL vial. The vial was sealed, and the contents were stirred overnight under nitrogen at 55 °C. The green product was isolated by filtration, washed with ether and pentane, and dried to give 0.378 g (55%) of product. The compound analyzed as the butanol adduct.

Complex 10. A solution of 0.200 g (1.10 mmol) of 2-(2,6-dimethylphenylthio)ethylamine **D** in 10 mL of cyclohexane was added to a mixture of 0.285 g (1.00 mmol) of monoimine **H** and 0.190 g (0.95 mmol) of $FeCl_2 \cdot 4H_2O$ in a 20 mL vial. The vial was sealed, and the contents were stirred overnight under nitrogen at 55 °C. The green product was isolated by filtration, and the green solid was redissolved in 5 mL of methylene chloride and refiltered to remove unreacted iron species. This redissolution was typically performed for complexes having lower yields, so as to remove insoluble materials. Removal of the CH_2Cl_2 from the filtrate gave 0.261 g (48%) of product. The compound analyzed as the monohydrate.

The other NNS precatalyst complexes were prepared similarly. Yields and additional characterization data are provided in Table 6.

Selected Syntheses for NNP-Ligated Iron Complexes. Complex 14. (2*E*)-2-[(2,6-Diisopropylphenyl)imino]acenaphthylen-1(2*H*)-one (1.24 g, 3.64 mmol), 1.00 g (3.50 mmol) of 2-(bis-(3,5-dimethyldiphenylphosphino))ethylamine, and 443 mg (3.49 mmol) of $FeCl_2$ powder were added to a scintillation vial with a stirbar. Then 17 mL of anhydrous *n*-butanol was added, the vial was sealed, and the reaction was stirred at 60 °C for 16 h. After cooling to ambient temperature, a green solid (2.07 g, 81%) was isolated by filtration and washed thoroughly with ether and pentane.

Complex 16. Monoimine **E** (299 mg, 1.00 mmol), 257 mg (1.00 mmol) of 2-(bis(2-methyldiphenylphosphino))ethylamine, and 121 mg (0.95 mmol) of $FeCl_2$ powder were added to a scintillation vial with a stirbar. Then 9 mL of anhydrous *n*-butanol was added, the vial was sealed, and the reaction was stirred at 55 °C for 6 h. After cooling to ambient temperature, a green solid (453 mg, 72%) was isolated by filtration and washed thoroughly with ether and pentane.

Complex 19. Monoimine **E** (598 mg, 2.00 mmol) and 242 mg (1.90 mmol) of $FeCl_2$ powder were added to a scintillation vial with a stirbar. In a separate vial, 482 mg (2.00 mmol) of 2-(dicyclohexylphosphino)ethylamine was dissolved in 13 mL of anhydrous *n*-butanol. The solution of the phosphinoamine was added to the first vial, the vial was sealed, and the reaction was stirred at 55 °C for 6 h. After cooling to ambient temperature, a green solid (887 mg, 72%) was isolated by filtration and washed thoroughly with ether and pentane.

The other NNP precatalyst complexes were prepared similarly. Yields and additional characterization data are provided in Table 6.

X-ray Crystallography. Complexes 2 and 4. Single crystals of **2** and **4** were mounted in thin-walled glass capillaries and transferred to a Bruker/Nonius MACH3S diffractometer equipped with graphite-monochromated Mo Kα radiation (λ = 0.71073 Å) for data collection at −100 °C. Relevant crystallographic information is given in Table 3. Unit cell constants were determined from a least-squares refinement of the setting angles of 25 intense, machine-centered reflections. Intensity data were collected using the $\omega/2\theta$ scan technique to a maximum

Table 6. Yield and Analytical Data for NNS- and NNP-Ligated Iron Complexes

		elemental analyses of complexes							
		calculated				found			
complex	% yield	%C	%H	%N	%O	%C	%H	%N	%O
2·H_2O	98	61.85	5.51	4.51		61.56	5.21	4.52	
3·H_2O	86	62.37	5.71	4.41		62.97	6.18	3.97	
4·H_2O	73	63.82	6.25	4.13	2.36	63.92	6.35	3.98	2.32
5·**BuOH**	55	57.16	5.46	3.70	2.12	56.94	5.17	3.77	1.28
6·H_2O	48	61.30	5.31	4.61		60.43	5.37	4.65	
7·H_2O	62	58.50	4.74	4.71		59.12	4.63	4.86	
8·H_2O	60	59.13	4.96	4.60		59.64	4.86	4.75	
9·H_2O	37	61.85	5.51	4.51	2.57	62.80	5.82	4.22	2.55
10·H_2O	48	60.72	5.10	4.72		60.53	5.00	4.31	
14	81	68.58	6.17	3.81	0	67.66	6.14	3.81	0.75
15	75	67.91	5.84	3.96	0	67.37	5.86	4.01	0.64
16	72	66.79	5.30	4.21	0	66.64	5.33	4.18	0.21
17·H_2O	40	64.59	5.27	4.18	2.39	63.71	5.05	3.93	2.39
18	74	66.00	7.14	4.05	0	65.04	7.34	3.97	1.04
19	72	64.73	6.67	4.31	0	64.53	6.76	4.20	0.54
20	41	64.27	6.50	4.41	0	63.83	6.50	4.31	0.72

2θ value of 50.02° (**2**) or 52.06° (**4**). Absorption corrections based on azimuthal scans were applied to the data, resulting in transmission factors ranging from 0.8997 to 0.6930 (**2**) or from 1.0 to 0.8258 (**4**). Corrections for crystal decay were not required. The intensity data were corrected for Lorentz and polarization effects and converted to structure factors using the CrystalStructure program.[35]

Space groups were determined on the basis of systematic absences and intensity statistics. Successful direct-methods solutions were calculated, which provided the positions of most of the non-hydrogen atoms directly from the E-map. The remaining non-hydrogen atoms were located after several cycles of structure expansion and full matrix least-squares refinement. Hydrogen atoms were added geometrically. All non-hydrogen atoms were refined with anisotropic displacement parameters except as noted below. Carbon-bound hydrogen atoms were refined as riding atoms with group isotropic displacement parameters fixed at 1.2*U*(eq) of the host carbon atom (for methylene and methine hydrogens) or 1.5*U*(eq) of the host carbon atom (for methyl hydrogens). The final difference maps were featureless, with the largest residual peak for **2** (1.065 $e^- Å^{-3}$) located 1.11 Å from Cl92, while the largest residual peak for **4** (1.055 $e^- Å^{-3}$) was located 0.99 Å from Fe1. Structure solution and refinement calculations were performed using the SHELXTL suite of programs[36] running on a Pentium PC.

The asymmetric unit of **2** contains two crystallographically independent complexes, two fully occupied molecules of CH_2Cl_2, and one-half-occupied molecule of CH_2Cl_2, which straddles an inversion center. The asymmetric unit of **4** contains a single molecule of CH_2Cl_2. One of the two *tert*-butyl groups of the ligand is disordered over two positions with refined occupancies of 0.703(11) and 0.297(11); a split atom model was applied to account for the rotational disorder. The low occupancy carbon atoms of this disordered *tert*-butyl group were modeled with isotropic displacement parameters.

Complex 14. A crystal (approximate dimensions 0.35 × 0.25 × 0.15 mm^3) of **14** was placed onto the tip of a 0.1 mm diameter glass capillary and mounted on a CCD area detector diffractometer for data collection at 173(2) K.[37] A preliminary set of cell constants was calculated from reflections harvested from four sets of 30 frames. These initial sets of frames were oriented such

(35) *CrystalStructure* V. 3.60; Rigaku Corporation and Rigaku/MSC, 2004.
(36) *SHELXTL* V. 6.10; Bruker AXS: Madison, WI, 2000.
(37) *SMART* V5.054; Bruker Analytical X-ray Systems: Madison, WI, 2001.

that orthogonal wedges of reciprocal space were surveyed. This produced initial orientation matrices determined from 165 reflections. The data collection was carried out using Mo Kα radiation (graphite monochromator) with a frame time of 30 s and a detector distance of 4.8 cm. A randomly oriented region of reciprocal space was surveyed to the extent of one sphere and to a resolution of 0.77 Å. Four major sections of frames were collected with 0.30° steps in ω at four different ϕ settings and a detector position of −28° in 2θ. The intensity data were corrected for absorption and decay (SADABS).[38] Final cell constants were calculated from 2912 strong reflections from the actual data collection after integration (SAINT).[39] Please refer to Table 3 for additional crystal and refinement information. The structure was solved and refined using Bruker SHELXTL.[40] The space group $I2/a$ was determined on the basis of systematic absences and intensity statistics. A direct-methods solution was calculated that provided most non-hydrogen atoms from the E-map. Full-matrix least-squares/difference Fourier cycles were performed, which located the remaining non-hydrogen atoms. All non-hydrogen atoms were refined with anisotropic displacement parameters. All hydrogen atoms were placed in ideal positions and refined as riding atoms with relative isotropic displacement parameters. The final full matrix least-squares refinement converged to $R_1 = 0.0380$ and $wR_2 = 0.1037$ (F^2, obsd data). The structure is the one suggested. One acetonitrile solvent molecule is found disordered in nearly 50:50 ratio, swinging between two positions roughly with the methyl carbon as fulcrum, where the angle between the two disordered positions is ∼58°. The occupancies of these were fixed at 50% once it was noticed that two of the disordered positions had a close nonbonded contact of the nitrile nitrogen atoms, respectively. The bond distances and ADPs for this pair were restrained for reasonable values. The $I2/a$ setting was chosen over the equivalent $C2/c$ setting since the β angle was nearer to normal for the I-centered setting.

Complex 18. A crystal (approximate dimensions 0.40 × 0.40 × 0.30 mm^3) of **18** was placed onto the tip of a 0.1 mm diameter glass capillary and mounted on a CCD area detector diffractometer for data collection at 173(2) K.[37] A preliminary set of cell constants was calculated from reflections harvested from three sets of 20 frames. These initial sets of frames were oriented such that orthogonal wedges of reciprocal space were surveyed. This produced initial orientation matrices determined from 151 reflections. The data collection was carried out using Mo Kα radiation (graphite monochromator) with a frame time of 40 s and a detector distance of 4.9 cm. A randomly oriented region of reciprocal space was surveyed to the extent of one sphere and to a resolution of 0.84 Å. Four major sections of frames were collected with 0.30° steps in ω at four different ϕ settings and a detector position of −28° in 2θ. The intensity data were corrected for absorption and decay (SADABS).[38] Final cell constants were calculated from 2843 strong reflections from the actual data collection after integration (SAINT).[39] Please refer to Table 3 for additional crystal and refinement information. The structure was solved and refined using Bruker SHELXTL.[40] The space group $P2_1/n$ was determined on the basis of systematic absences and intensity statistics. A direct-methods solution was calculated that provided most non-hydrogen atoms from the E-map. Full-matrix least-squares/difference Fourier cycles were performed, which located the remaining non-hydrogen atoms. All non-hydrogen atoms were refined with anisotropic displacement parameters. All hydrogen atoms were placed in ideal positions and refined as riding atoms with relative isotropic displacement parameters. The final full-matrix least-squares refinement converged to $R_1 = 0.0554$ and $wR_2 = 0.1422$ (F^2, all data). The structure is the one suggested. There are two molecules of interest in the asymmetric unit along with one acetonitrile solvent molecule of crystallization. It appears there is some minor disorder of the cyclohexyl group C7A−C12A that cannot be modeled. Most warnings of merit in the CHECKCIF output are related to the minor disorder of this group.

Acknowledgment. The authors thank Chevron Phillips Chemical Company for permission to publish these results and for their generous support of this work at the University of Wisconsin−Eau Claire. M.J.C. also acknowledges the University of Wisconsin−Eau Claire Office of Research and Sponsored Programs for financial support. In addition, we thank Dr. Victor G. Young, Jr. and the X-ray Crystallographic Laboratory at the University of Minnesota for determining the X-ray crystal structures of **14** and **18**.

(38) An empirical correction for absorption anisotropy: Blessing, R. *Acta Crystallogr.* **1995**, *A51*, 33–38.

(39) *SAINT+* V6.45; Bruker Analytical X-Ray Systems: Madison, WI, 2003.

(40) *SHELXTL* V6.14; Bruker Analytical X-Ray Systems: Madison, WI, 2000.